Effect of Platform Configurations and Environmental Conditions on the Performance of Floating Solar Photovoltaic Structures

M I Jifaturrohman[1,], T Putranto[1], D Setyawan[1], L Huang[2], I K A P Utama[1*]

ABSTRACT

The growth and development of floating solar photovoltaic (FPV) power plants is a prominent topic within renewable energy technology. One reason contributing to this desired technology design concept is the possibility of land acquisition issues, whereas the usage of the ocean provides a greater technical alternative area. The objective of the research is to present an innovative design for a floating structure, focusing on investigating and comparing the seakeeping performance of several hull configurations: catamaran, trimaran, quadrimaran and pentamaran. The final computational simulation results indicate a linear negative trend in the motion response graphs, particularly in specific significant response values for heave (Global Z), roll (Global RX), and pitch (Global RY), as the hull configuration increases.

KEY WORDS

CFD; Floating photovoltaic; Multi-hull; Renewable energy; Seakeeping characteristics.

NOMENCLATURE

AP	=	Aft Perpendicular	H	=	Height of FPV
Aγ	=	Normalising Factor	ha	=	Hectare
B	=	Breadth	HDPE	=	High-Density Polyethylene
B1	=	Demihull Breadth	Hs	=	Significant Wave Height
Cb	=	Block Coefficient	IEA	=	International Energy Agency
CFD	=	Computational Fluid Dynamics	IESR	=	Institute for Essential Services Reform
CFPP	=	Coal-Fired Power Plants	Ixx	=	Inertia moment – X-Axis
CH_4	=	Methane	Iyy	=	Inertia moment – Y-Axis
CL	=	Center Line	Izz	=	Inertia moment – Z-Axis
CO_2	=	Carbon Dioxide	JONSWAP	=	Joint North Sea Wave Project
CoG	=	Center of Gravity	KB	=	Keel to Buoyancy
Cp	=	Prismatic Coefficient	kW	=	Kilowatt
FP	=	Forward Perpendicular	Kxx	=	Radii of gyration – X Axis
FPV	=	Floating Photovoltaic	Kyy	=	Radii of gyration – Y Axis
g	=	Acceleration due to Gravity	Kzz	=	Radii of gyration – Z Axis
GHG	=	Greenhouse gas	LCB	=	Longitudinal Center of Buoyancy
GHI	=	Global Horizontal Irradiation	LCG	=	Longitudinal Center of Gravity
GWp	=	Giga Watt peak	LoA	=	Length over All

[1] Department of Naval Architecture, Faculty of Marine Technology, Institut Teknologi Sepuluh Nopember, Surabaya, 60111, Indonesia.

[2] School of Water, Energy, and Environmental, Cranfield University, Bedford, MK 43 0AL, UK.

* Corresponding Author: *kutama@na.its.ac.id*

m	=	meter	ω	=	Angular Frequency (Wave Frequency)
MWp	=	Mega-Watt peak	S_J	=	JONSWAP's Wave Spectrum
N_2O	=	Nitrous Oxide	S_{PM}	=	Pierson-Moskowitz Wave Spectrum
NJR	=	New Jersey Resources Corporation	S_ζ	=	Wave Spectrum
R^2	=	Validity Error Values – R Squared	m_0	=	Area under the Response Spectrum Curve
RAOs	=	Response Amplitude Operators	∇	=	Laplace Operator
S	=	Spacing of FPV	ζ_{k0}	=	Amplitude of Motion in a Specific Mode
T	=	Draft of FPV	ζ_0	=	Wave Amplitude
Tp	=	Peak Wave Period	$S_{\zeta r}$	=	Response Spectra
UV	=	Ultra-Violet	ζ_s	=	Significant Amplitude
ϕ	=	Potential Velocity Function	γ	=	Non-dimensional peak shape parameter
Δ	=	Displacement	φ	=	Wave Heading
σ	=	Spectral Width Parameter			

INTRODUCTION

Indonesia strives to achieve a 23% renewable share of energy in the nation's overall energy composition within the next year based on the Minister of Energy and Mineral Resources of the Republic of Indonesia (2021), as depicted in Figure 1. a.

The high dependency on coal has the potential to result in a significant increase in greenhouse gas (GHG) emissions. As an example, by the end of 2021, the Institute for Essential Services Reform, IESR (2022) determined that the greenhouse gas emission profile in Indonesia was primarily comprised of CO_2, with a contribution of 93.10%. Following together was CH_4 at roughly 5.90%, whilst the remaining 1.00% is identified as N_2O following in Figure 1. b. Even though methane (CH_4) contributes less to emissions than CO_2, it can cause emissions which are as high as 29.80 times higher.

Furthermore, another extensive review of IEA (2022) data reveals that coal combustion, specifically in coal-fired power plants (CFPPs), is responsible for a considerable 72.10% of methane (CH_4) emissions. As shown in Figure 1c, the oil and gas industry contributes 23.40% of these emissions, with the remaining 4.50% going to the bioenergy sector.

The Existing Indonesia's Power Plant Conditions in 2022

(a)

(b)

(c)
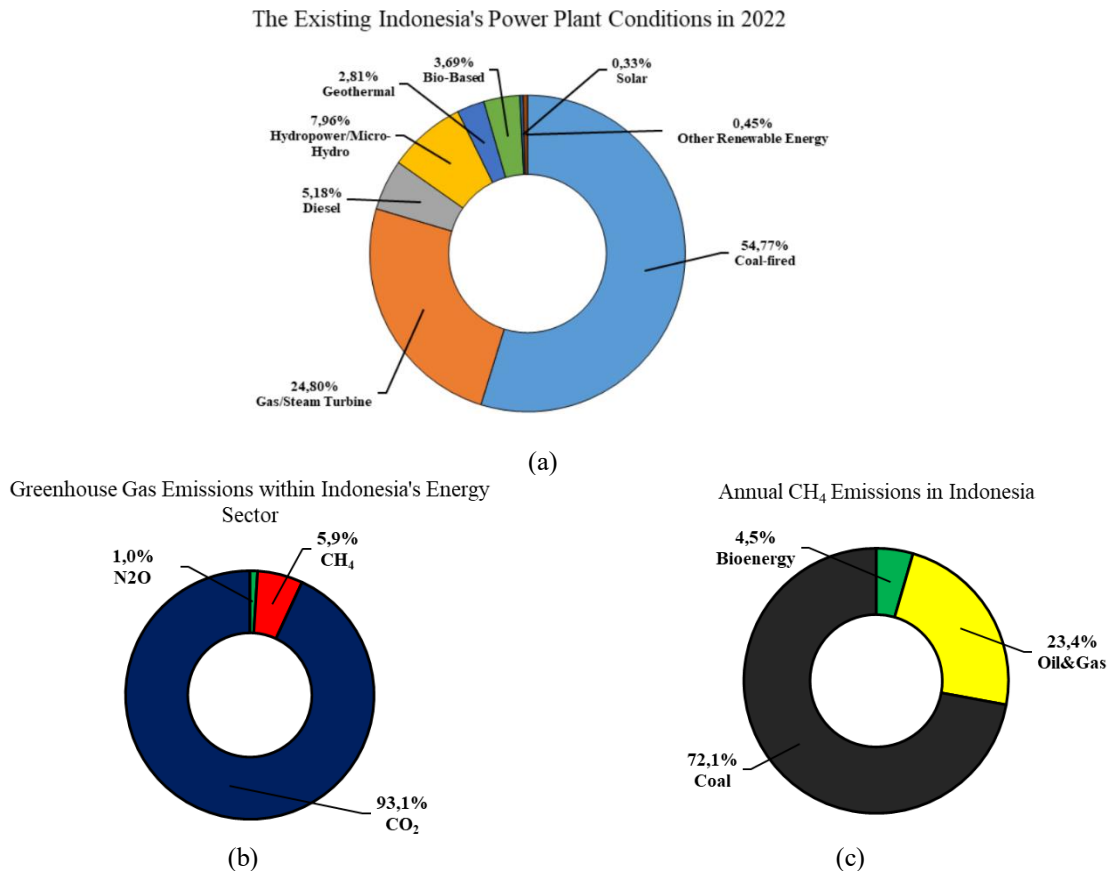
Figure 1. (a) The Ratio of Power Plant Conditions in Indonesia in 2022, (b) Greenhouse Gas Emissions within Indonesia's Energy Sector, (c) Annual CH_4 Emissions in Indonesia

Therefore, in a proactive action, the Indonesian government has issued a document Presidential Regulation 112 (2022), aiming to expedite the development of renewable energy for electricity supply. This regulation represents the gradual phase-out of coal-fired power plants (CFPPs). However, data from the Directorate General of Renewable Energy and Energy Conservation (2022), indicates that the share of Renewable Energy (RE) in the national energy mix was 12.16% in 2021, with a slight increase of 0.12% in 2022, which should be valued at 12.30%. Figure 2 illustrates the comparison of the percentage between the planned actions and the realization share mix of renewable energy implementation with a total target of 23% in the monitoring year 2022.

Plan vs Realization of Renewable Energy in 2022 with a National Target of 23% Renewable Energy Mix
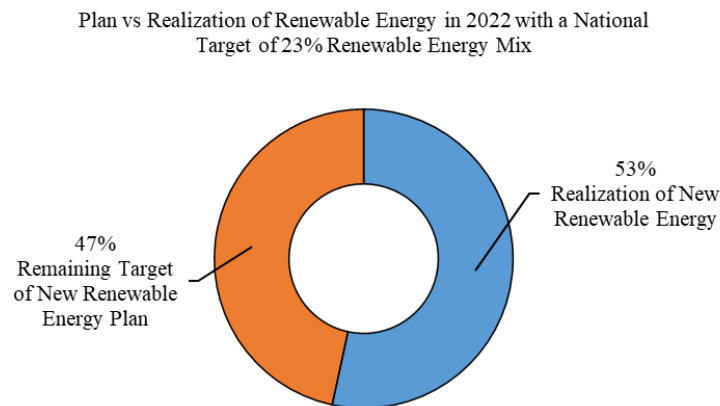
Figure 2. Realization vs Remaining Target of the Renewable Energy Plan in 2022

Approaching the year 2025, the State Electricity Company emphasizes the crucial role of expanding hydroelectric and geothermal power plants to achieve the 23% target in the national energy mix, as both sources can generate a significant energy by the Minister of Energy and Mineral Resources of the Republic of Indonesia (2021). However, these government projects have faced delays due to challenges related to land acquisition, environmental exploration, social concerns, and the high investment required. As a result, it is critical to take proactive actions toward discovering alternate renewable energy sources. An example is the deployment of solar energy converter systems.

Additionally, as highlighted by Shi et al., (2023), Solar energy is ecologically favourable, prominent, and widely distributed, warranting robust development. The solar photovoltaic (PV) system is a popular technology for directly converting solar energy into electricity using the photogenerated power effect of PV cells. Its wide range of uses includes both on-grid and off-grid power systems.

Implementing large-scale operations in photovoltaic (PV) power plants is a considerable difficulty due to the substantial land required for installation as explained by Sreenath et al., (2020). Then, as predicted by Rosa-Clot & Tina (2018), Land-based solar power facilities have an average demand of 0.50-0.70 MWp/ha. Furthermore, Pimentel & Branco (2018) explained that the forest destruction, extinction of birds due to habitat loss, erosion, runoff, and microclimate changes are some of the issues that arise throughout the installation and generation stages. Then a brief overview by Wang & Lund (2022), presents that in dealing with these challenges, researchers are actively investigating water-based PV systems, which include both fixed and floating PV (FPV) technologies from an offshore perspective. This novel technique is emerging as a promising alternative, searching to tackle the energy demand while limiting the environmental impact (Shi et al., 2023)

The fixed PV systems model, as described by Shi et al., (2023), illustrates that solar panels are secured to the seabed using pile foundations. However, the economic implications of this bottom-fixed technique reduce with increasing water depth, due to the substantially higher cost of piling. As a result, Rosa-Clot & Tina (2018) and World Bank Group (2019), give alternative solutions that are explored for deep water applications offshore, often using floating PV (FPV) systems. These FPV systems typically represent floaters or pontoons, PV modules, mooring systems, and cables as stated by Rosa-Clot et al., (2010) and Sen et al., (2015).

Over the past ten years, there has been an essential global study on floating photovoltaic (FPV) technology. The Aichi Project in Japan, with a capacity of 20 kW, represented the introduction of the first pilot FPV technology to the world in 2007, as may be noticed by Choi et al., (2016). Subsequently, the World Bank Group (2019) confirmed that in 2008, the first commercially operating FPV plant was presented in California, USA, with a capacity of 175 kW. Initially, these two initial projects are specifically designed for small-scale research projects. Trapani & Santafé (2015), confirmed that in 2015, Japan launched its first large-scale FPV plant, with a capacity of 7.55 MWp, followed by Boersma et al., (2019) revealed that a 40 – MWp plant was introduced in China in 2017. With the financial support of the African Development Bank and Clinton Foundation, Seychelles accomplished a historic milestone by establishing a 4 MW FPV plant in 2018 then becoming the first African nation to create history in FPV technology as explained by Beetz, (2018).

Proceeded into the year 2019, the Korea Energy Agency (2022) informed that the Korean rural community corporation was established to install 280 MW of FPV plants, whereas France built a 17 MW FPV system (Kenning, 2018). In the opening years of 2022, Shandong province in China delivered its largest FPV plant to the grid system, with a capacity of 320 MW (Lindholm et al., 2022). Furthermore, particularly in Indonesia, in collaboration with Masdar, is looking into a 60.00 MW FPV project to achieve 23% renewable energy by 2025 and 31% by 2030, with a significant milestone 145 MW project executed on a 250-hectare water area (Masdar, 2023). Singapore-based company "Sunseap" is developing a large 2.20 GW FPV in the Batam reservoir, expected completed by 2024 (Silalahi et al., 2021). Singapore has impressive goals to develop the world's biggest offshore FPV plant with a capacity of 2.00 GW by 2030 in its renewable energy sector (Liu et al., 2020). Additionally, the United States currently discovering the largest FPV project in progress, an 8.90 MW installation managed by New Jersey Resources Corporation (NJR) Clean Energy Ventures in Millburn, New Jersey. (Islam et al., 2023). Table 1 which follows provides further information and details on the ten largest FPV projects undertaken globally starting in 2020.

Table 1. The ten most extensive floating photovoltaic (FPV) projects worldwide

No	Country	Electric Capacity	Location	Provider / Investor	Years	Ref
1	Indonesia	2200 MW	Duriangkang reservoir, Batam Island	Sunseap, BP Batam	2024-2025	(Reuters, 2021)
2	South-Korea	2100 MW	Saemangeum floating solar energy project	SK E&S, Ocean Sun Hanwa Q Cells	2025-2030	(Frost&Sullivan, 2024)
3	India	600 MW	Omkareshwar reservoir, Madhya Pradesh	Tender process on going	2023-2024	(Frost&Sullivan, 2024)
4	China	550 MW	Wenzhou, Zhejiang Province	Chint Group	2021	(Emiliano Bellini, 2022)
5	Vietnam	500 MW	Laly hydropower reservoir, Dong Nai	Blueleaf Energy Asia	2021	(Japan International Cooperation Agency (JICA), 2020)
6	China	320 MW	Changhe and Zhouxiang reservoirs in Cixi	Hangzhou Fengling Electricity Science Technology	2020	(Frost&Sullivan, 2024)
7	Laos	240 MW	Nam Theun 2 hydropower plant, Khammouane	Electricté De France - EDF	2024	(Amir Garanovic, 2021)
8	Taiwan	181 MW	Chenghua County	Chenya Energy	2020	(Enerdata, 2020)
9	Indonesia	145 MW	Cirata, West Java	Masdar Solar Energy	2022	(Frost&Sullivan, 2024)
10	Thailand	45 MW	Sirindhorn Dam, Chanin Saleechan	B.Grimm Power, Energy China	2021	(Tom Kenning, 2019)

Table 1 shows Indonesia's ability to achieve a significant position among the top ten Floating Photovoltaic (FPV) projects globally supported by the highest potential Global Horizontal Irradiation (GHI), reaching up to 4.80 kWh/m2, as reported by (Silalahi et al., 2022), and represented in the subsequent Figure 3, when contrasted with other countries. This observation suggests that the adoption of FPV technology in Indonesia presents substantial and expansive opportunities, emphasizing the need for strategic planning to harness this potential for the future.

Global Horizontal Irradiation, GHI (kWh/m^2)

4,5 Singapore
4,8 Indonesia
2,9 Germany
3,6 Japan
4,1 China
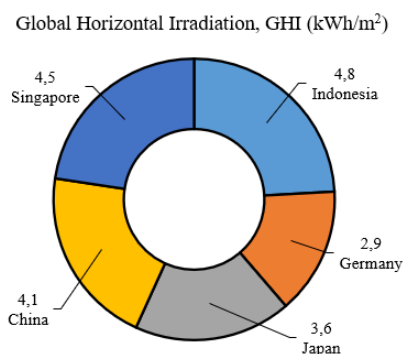
Figure 3. Global Horizontal Irradiation (GHI)

During the design process of a Floating Photovoltaic (FPV) system, a critical part is the floating structural component. It plays a crucial part in ensuring the system's buoyancy and stability. Following a research study by Sahu & Sudhakar (2019), the floating structure is often made of non-hazardous, UV light-resistant, and maintenance-free plastic materials recognised for their high tensile strength, for example, High-Density Polyethylene (HDPE). Several studies from Oliveira-Pinto & Stokkermans (2020); World Bank Group (2019) and Claus & López (2022) show that applying HDPE has numerous benefits, including a simple and easily implemented construction. Its lightweight characteristic contributes to reducing tension on the overall structure in response to offshore hydrodynamic pressures, and the use of minimum metal reduces susceptibility to corrosion. Furthermore, HDPE provides cost-effective beneficial effects when compared to other materials such as concrete (Mittal et al., 2017) and steel (Cazzaniga et al., 2017)

Taking these various factors into consideration, this study proposes a novel approach for floaters by utilizing the geometric shape of High-Density Polyethylene (HDPE) hulls. This material has several advantages, including resistance to the sea environment and protection against UV degradation effects. The research focuses on innovative floater design configurations in catamaran, trimaran, quadrimaran, and pentamaran. The impact of the hull configuration, administered as an initial design parameter, will be investigated by Computational Fluid Dynamics (CFD) simulations under the JONSWAP wave spectrum, including various sea-state situations.

The paper is organized as follows: **Section 2** describes the problem characterisation for the original concept of floating hull constructions. **Section 3** provides an extensive overview of the research methodology, as well as technical details about the Computational Fluid Dynamics (CFD) numerical setup. **Section 4** advances further into the CFD numerical simulation findings, investigating the effect of hull configuration on motion characteristics. Finally, **Section 5** provides a summary of the study, emphasizing its important findings.

PROBLEM CHARACTERIZATION

A multi-hull construction with several configurations starting from the catamaran (2 hulls), trimaran (3 hulls), quadrimaran (4 hulls), and pentamaran (5 hulls) is proposed. These hulls are identical geometric shapes and sizes, arranged in parallel to form an integrated structure (single-array) designed for energy farming. This numerical study considers several factors, including independent variables, dependent variables, and control variables. In a numerical/experimental study, the researcher manipulates or changes the independent variables to determine how they affect the dependent variables. Dependent variables are measured or observed in reaction to changes in independent variables, indicating the predicted outcomes of the numerical/experimental study. In numerical/experimental studies, control variables remain constant to ensure that changes in independent variables are the cause of observed effects on dependent variables. Table 2 describes the individual variables utilized in this numerical investigation.

Table 2. Utilized variables

Independent Variables	Dependent Variables	Control Variable

• Sea-State [Hs]
   ○ Sea-State 1 [0.1 m]
   ○ Sea-State 2 [0.5 m]
   ○ Sea-State 3 [1.25 m]
   ○ Sea-State 4 [2.50 m]
 • Wave Heading
   ○ 0 Degree [Head Sea]
   ○ 45 Degree [Oblique Sea]
   ○ 90 Degree [Beam Sea]
 • Hull Configuration
   ○ Catamaran
   ○ Trimaran
   ○ Quadrimaran
   ○ Pentamaran
	• Significant heave response ($\zeta_{s\,Global\,Z}$)
	 • Significant roll response ($\zeta_{s\,Global\,RX}$)
	 • Significant pitch response ($\zeta_{s\,Global\,RY}$)
		• LoA
		 • Breadth Demihull
		 • Spacing
		 • Height
		 • Draft

The dominant pure oscillatory response motions, particularly heave, rolling, and pitching characteristics in regular waves, will be determined by evaluating the free-floating conditions for all proposed design models. The results will be shown in a graph of Response Amplitude Operators (RAOs), where the frequency parameter is indicated on the horizontal axis (X-absis) and the ratio of motion amplitude in a specific mode to the wave amplitude is represented on the vertical axis(Y-ordinate), as explained by Djatmiko (2012).

As a result, the motion quality values for each proposed design will be presented as a representation of a curve, with the x-axis representing the type or number of hull configurations for the floaters and the y-axis representing the floating structure motion quality values (heave, roll, and pitch) for a specific sea-state. The trends of the scatter graph for each simulation result point

will be represented by the equation of a line that corresponds to the validity error values - R squared (R^2) within the value that comes closest to 1.

METHODOLOGY

This numerical solution is based on a Computational Fluid Dynamics (CFD) simulation. The following subsection includes data for each proposed design with initial main principal dimensions, along with electrical capacity and weight distribution calculations then followed by a general layout. The seakeeping performance is evaluated by significant response spectra ($\zeta_{s[Z]}$, $\zeta_{s[RX]}$, $\zeta_{s[RY]}$,) , using further stochastic computations to calculate the area under the spectrum curve for specific sea situations.

Model Description & Initial Calculation

The stated numbers for floater hull dimensions are identical for each proposed design configuration, indicating that the addition of hull different forms is carried out by replicating the shape of the previous hull design laterally following Figure 4.

a

b

c

d
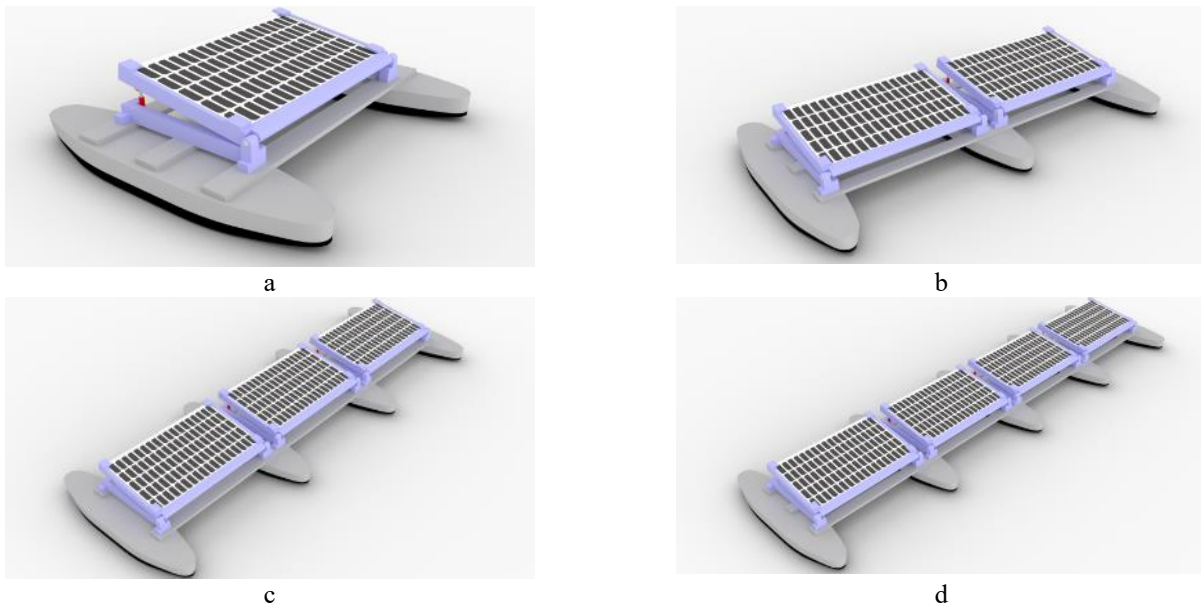
Figure 4. Novel design of hull geometry adaptation for FPV: (a) Catamaran, (b) Trimaran, (c) Quadrimaran, (d) Pentamaran

The main dimensions related to the hydrostatic properties of each design are tabulated in Table 3. It should be noted that, due to the identical values of the hull shape dimensions, this will result in hydrostatic properties of the identical FPV floating structure, except for the total width and displacement values of the FPV structure.

Table 3. Main principles dimension

Parameter	Catamaran	Trimaran	Quadrimaran	Pentamaran	Units
Length over All (LoA)	3.24	3.24	3.24	3.24	m
Breadth (B)	3.54	6.34	9.14	11.94	m
Height (H)	0.30	0.30	0.30	0.30	m
Draft (T)	0.12	0.12	0.12	0.12	m
Demihull Width (B1)	0.74	0.74	0.74	0.74	m
Spacing (S)	2.80	2.80	2.80	2.80	m
Hydrostatic properties					
Displacement (Δ)	437.31	655.31	874.74	1094.17	kg
Block coefficient (Cb)	0.75	0.75	0.75	0.75	-
Prismatic coefficient (Cp)	0.76	0.76	0.76	0.76	-
Keel to buoyancy (KB)	0.06	0.06	0.06	0.06	m
Longitudinal Center of Buoyancy (LCB) from AP	1.62	1.62	1.62	1.62	m

Table 4 shows the total installed power capacity for each proposed model, as well as the characteristics of the solar panel technology used.

Table 4. PV system specification and total power generation capacity

Parameter	Value	Unit	Remarks
PV capacity	665	Watt peak (Wp)	
Module efficiency	21.40	%	
Length of PV	2.38	m	(CSI Solar Co. Ltd, 2021)
Width of PV	1.30	m	
PV module weight	34.40	kg	
Total generating capacity			
Catamaran	665	Watt peak (Wp)	These calculations are
Trimaran	1330	Watt peak (Wp)	based on the maximum
Quadrimaran	1995	Watt peak (Wp)	capacity of the considered
Pentamaran	2660	Watt peak (Wp)	PV system technology

Governing Equations

The CFD simulation software's governing equation assumed a homogeneous, inviscid, irrotational, and incompressible fluid, as outlined by (Haug et al., 2018). This assumption aims to identify the potential velocity function, which serves as a criterion for determining fluid characteristics like velocity and pressure. The computation of Response Amplitude Operators (RAOs) within the Boundary Element Method (BEM) techniques were performed using (Ansys, 2019). The potential velocity can be expressed as equation (1), where i, j, and k represent unit vectors along the x-, y-, and z-axes, respectively.

$$V = \nabla_\phi = \frac{\partial \phi}{\partial x} i + \frac{\partial \phi}{\partial y} j + \frac{\partial \phi}{\partial z} k \tag{1}$$

Under the assumption that the fluid remains incompressible – implying a consistent mass within the flow entering and leaving a control surface – the Laplace equation is formulated by the following expression (2).

$$\nabla^2 \phi = \frac{\partial u}{\partial x} + \frac{\partial v}{\partial y} + \frac{\partial w}{\partial z} = 0 \tag{2}$$

Subsequently, to ensure compliance with the continuity equation, every potential velocity solution should be accompanied by the non-rotation condition outlined in equation (3). In simpler terms, an irrotational fluid is one in which the vorticity vector is uniformly zero across the entire fluid.

$$\omega_v = \nabla^2 \times V = 0 \tag{3}$$

In this scenario, fluid does not pass through the surface of a fixed body in motion. This condition indicates the impermeability of the object and is expressed in equation (4).

$$\frac{\partial \phi}{\partial n} = 0 \tag{4}$$

While equation (4) indicates the impermeability of a fixed body, such as the seabed, with n representing a normal vector pointing from the seabed and extending into the fluid, equation (5) expands this concept for a moving body with a velocity V

$$\frac{\partial \phi}{\partial n} = V . n \tag{5}$$

The kinematic free-surface condition states that in the presence of small waves, fluid particles at the surface are expected to remain on the free surface. Furthermore, the dynamic free-surface condition requires that the water pressure at the free surface becomes equal to a constant atmospheric pressure. The following equation (6) expresses the simplified and linearized formulations for the kinematic and dynamic free-surface conditions, which use linear theory and assume small waves, zero current, and zero forward speed of the body.

$$\frac{\partial^2 \zeta}{\partial t^2} + g \frac{\partial \phi}{\partial z} = 0 \quad on \ z = 0 \tag{6}$$

In the end, as the vessel interacts with the waves, the potential velocity becomes an instrument for representing the wave flow field around the hull sections. Furthermore, the potential velocity is critical in computing the fluid force applied on the hull section, as well as determining hull motion and wave force. Consequently, the potential velocity generated by external waves can be combined using the method described in (7).

$$\phi = \phi_i + \phi_r + \phi_d \tag{7}$$

ϕ_i, ϕ_r, ϕ_d representing the potential functions for the incident wave, radiation wave, and diffraction wave, respectively. ϕ_i is computed using Airy linear theory, while the derivation of ϕ_r and ϕ_d relies on the application of diffraction theory. In diffraction theory, the potential function is determined by solving the Laplace equation, considering relevant boundary conditions, and subsequently calculating the pressure and resulting forces acting on the body. Additionally, pressure is extracted using the Bernoulli equation, and the potential function is determined. In conclusion, the integration of pressure over the entire wet surface area produces wave excitation forces, which are then utilized in the AQWA software.

Response Amplitude Operators (RAOs)

The Response Amplitude Operator (RAO) is a function of the dynamic motion of a structure induced by waves within a specific frequency range. RAO serves as a tool to convert wave forces into the dynamic motion response of the structure. Translation and rotational RAOs are described by equations (8) – (9).

$$RAO_{(k=x,y,z)} = \frac{\zeta_{k0}}{\zeta_0} \tag{8}$$

$$RAO_{(k=\theta,\phi,\psi)} = \frac{\zeta_{k0}}{\left(\frac{\omega^2}{g}\right)\zeta_0} \tag{9}$$

Calculation of Wave Spectral

JONSWAP's wave spectrum formulation is a modified version of the Pierson-Moskowitz spectrum with integrating parameters to accommodate the characteristics of waves in enclosed waters or island environment Djatmiko (2012) Therefore, it is suitable for application in Indonesia's archipelago with the following equation (10) – (14) based on DNV-GL recommendation Det Norske Veritas (2010)

$$S_J(\omega) = A_\gamma S_{PM}(\omega)\gamma^{exp\left[-0.5\left(\frac{\omega-\omega_p}{\sigma\omega_p}\right)^2\right]} \tag{10}$$

$$S_{PM}(\omega) = \frac{5}{16}.H_s^2\omega_p^4.\omega^{-5}exp\left[-\frac{5}{4}\left(\frac{\omega}{\omega_p}\right)^{-4}\right] \tag{11}$$

$$\omega_p = \frac{2\pi}{T_p} \tag{12}$$

$$A_\gamma = 1 - 0.287\ln(\gamma) \tag{13}$$

$$\sigma = 0.07 \ for \ \omega \leq \omega_p \ \mathbf{or} \ \sigma = 0.09 \ for \ \omega > \omega_p \tag{14}$$

Where, $S_J(\omega)$ is the JONSWAP spectrum, $S_{PM}(\omega)$ is the Pierson-Moskowitz spectrum, ω_p is the angular spectral peak frequency, T_p is the spectral peak period, H_s is the significant wave height, A_γ is the normalizing factor, γ is the non-dimensional peak shape parameter, and σ is the spectral width parameter.

Calculation of Responses Spectral

The responses of a floating structure in irregular waves shall be obtained by correlating the RAO with the wave spectrum within transforming wave energy into response energy with the following equation (15). Subsequently, the amplitude significant response is calculated as equation (16).

$$S_{\zeta r}(\omega) = RAO^2 \times S_\zeta(\omega) \tag{15}$$

$$\zeta_s = 2\sqrt{m_0} \tag{16}$$

Where $S_{\zeta r}$ (ω) is the response spectrum, S_ζ (ω) is the waves spectrum and m_0 is the area under the response spectrum curve as shown in the following equation (17).

$$m_0 = \sum_{n=1}^{\infty} S_\zeta(\omega)\delta\omega = \int_0^{\infty} S_\zeta(\omega)d\omega \tag{17}$$

3-D Diffraction CFD Simulation Setup

The three-dimensional (3D) models of floating structures were developed using the Maxsurf modeler by Bentley System (2022). Subsequently, the 3D model was exported in .step format through Rhinoceros software to conduct seakeeping analysis using Ansys Aqwa. The statistical validation between Ansys Aqwa and the baseline for manual calculations was required to stay within a 2% threshold for all considerations, as detailed in the results presented in Table 4 (a) – (d) as recommended by Suastika et al., (2021)

Table 5. Statistical validation: (a) catamaran, (b) trimaran, (c) quadrimaran, (d) pentamaran

(a)

Parameter	AQWA	Manual Calculation	Difference (%)
Hydrostatic properties			
Displacement Δ (ton)	442.80	437.31	1.25
Water plane area (m^2)	3.86	3.86	0.21
Longitudinal center of gravity, LCG (m) from AP – CL	1.62	1.62	0.00
Inertia Properties			
Inertia moment – X Axis, Ixx (kg.m^2)	584.36	577.09	1.26
Inertia moment – Y Axis, Iyy (kg.m^2)	204.81	202.26	1.26
Inertia moment – Z Axis, Izz (kg.m^2)	779.81	770.12	1.26

(b)

Parameter	AQWA	Manual Calculation	Difference (%)
Hydrostatic properties			
Displacement Δ (ton)	663.40	655.31	1.23
Water plane area (m^2)	5.80	5.79	0.22
Longitudinal center of gravity, LCG (m) from AP – CL	1.62	1.62	0.00
Inertia Properties			
Inertia moment – X Axis, Ixx (kg.m^2)	2696.87	2663.35	1.26
Inertia moment – Y Axis, Iyy (kg.m^2)	299.65	295.81	1.30
Inertia moment – Z Axis, Izz (kg.m^2)	2982.29	2944.16	1.30

(c)

Parameter	AQWA	Manual Calculation	Difference (%)
Hydrostatic properties			
Displacement Δ (ton)	884.12	874.74	1.07
Water plane area (m^2)	7.74	7.72	0.21
Longitudinal center of gravity, LCG (m) from AP – CL	1.62	1.62	0.00
Inertia Properties			
Inertia moment – X Axis, Ixx (kg.m^2)	7241.88	7165.42	1.07
Inertia moment – Y Axis, Iyy (kg.m^2)	436.94	431.83	1.18
Inertia moment – Z Axis, Izz (kg.m^2)	7657.56	7575.05	1.09

(d)

Parameter	AQWA	Manual Calculation	Difference (%)
Hydrostatic properties			
Displacement Δ (ton)	1104.23	1094.16	0.92
Water plane area (m²)	9.67	9.67	0.20
Longitudinal center of gravity, LCG (m) from AP – CL	1.62	1.62	0.00
Inertia Properties			
Inertia moment – X Axis, Ixx (kg.m²)	15018.96	14883.71	0.91
Inertia moment – Y Axis, Iyy (kg.m²)	542.62	537.30	0.99
Inertia moment – Z Axis, Izz (kg.m²)	15536.47	15392.39	0.94

Furthermore, the motion characteristics are the combination of the mass properties and hull surface geometry of the floating structure. The mass properties such as inertia values and center of gravity (CoG) indicate how resistant a body is to changes in its rotational state. The mass properties are defined in Ansys Aqwa as a "point mass" with automatically calculated in mass and only input in radius gyration as can be seen Table 5.

Table 6. Radii of gyration of floating structures

Component	Catamaran (m)	Trimaran (m)	Quadrimaran (m)	Pentamaran (m)
K_{xx} (X-Axis)	1.15	2.02	2.86	3.69
K_{yy} (Y-Axis)	0.68	0.67	0.70	0.70
K_{zz} (Z-Axis)	1.33	2.12	2.94	3.75

The generating mesh provides to calculation of pressures and forces on each number element in hull surface geometry (Bosma et al., 2012). A finer mesh was used in interface between wet and dry surface region. Both of floating were meshed as shown in Figure 4.

a

b

c

d
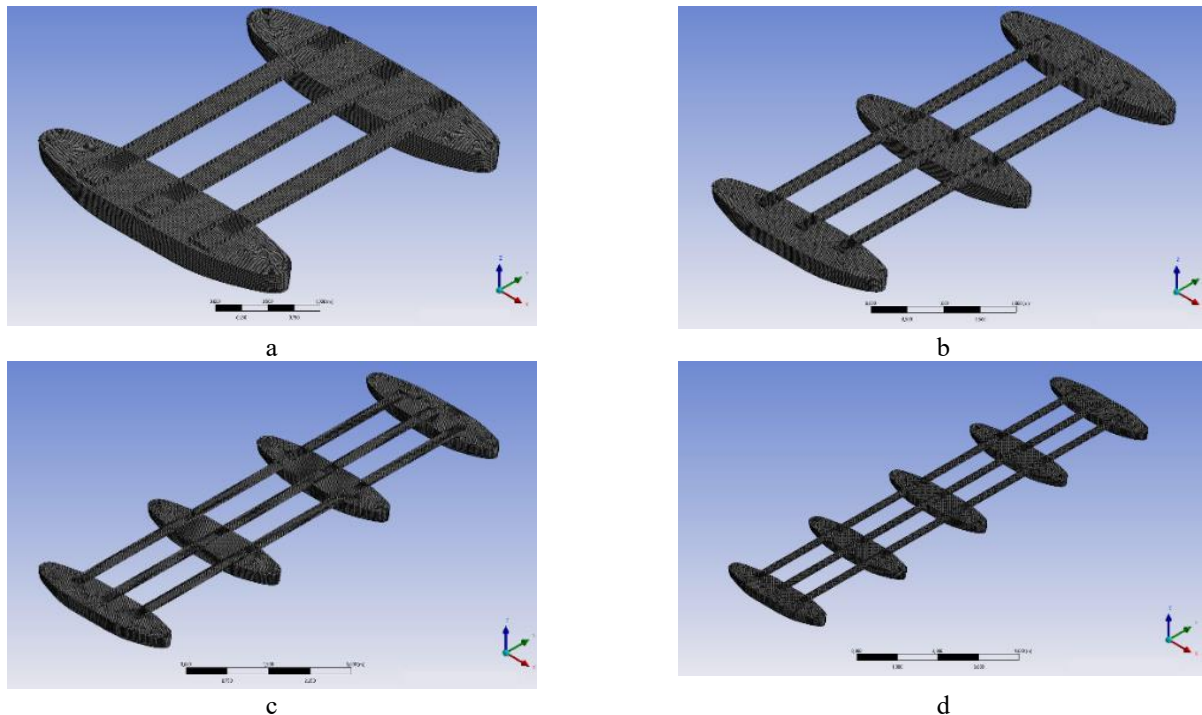
Figure 5. Mesh visualization: (a) Catamaran, (b) Trimaran, (c) Quadrimaran, (d) Pentamaran

RESULT AND DISCUSSION

The results and discussions in this paper are divided into subsections: a key point of the fundamental proposed design, Response Amplitude Operators (RAOs) and JONSWAP's wave spectra under various sea states, including structural response spectra within stochastic values.

The main recommended design component emphasizes the importance of selecting hull-shaped floater concepts in PV technology, covering from catamaran to pentamaran shapes. This subsection examines several of the advantages of this multi-hull design in depth.

In the RAOs subsection, all graphs related to motion analysis in heave, roll, and pitch modes for each proposed design model are explained in the frequency range of 0.05 – 3.00 rad/sec. Explanations for the heave RAO graph will be presented for headings φ = 0, φ = 45, and φ = 90 degrees. The roll RAO graph is subsequently clarified for headings φ = 45 and φ = 90 degrees. The pitch RAO graph is described at headings of φ = 0 and φ = 45 degrees.

The significant response value of oscillatory pure motions subsection describes various aspects, including significant wave height values under each sea-state condition, and the visualization of JONSWAP wave spectra, followed by several graphical representations of motion quality calculations for each mode and sea-state condition for each proposed model.

A Key Point of the Fundamental Proposed Design

The floater structure, as a form of buoyant force, must be designed to withstand vertical and horizontal loads. The vertical load is less substantial than anticipated, as evidenced by the lightweight proportion of this FPV innovation design, which is just approximately 38% of the total displacement capacity, indicating that this technology was created with minimalism and lightness. Furthermore, horizontal cyclic loads such as wind, wave, and current loads must be considered because the technology will be utilized in nearshore locations (Liu et al., 2018). However, presently, HDPE blocks are commonly used in the implementation of FPV technology in lakes with generally calm water conditions – related to restricted limited wind fetch generating waves and mountains surrounded area (Allsop et al., 2018; Gudrun Sigtryggsdottir, 2022). Typically, certain designs involve only segments of the HDPE blocks, which are then arranged on the water surface to provide adequate buoyancy and serve as a platform for solar panel technology. Shifting the perspective toward nearshore areas is aimed at harnessing a significantly larger technical space compared to utilizing reservoirs – which are typically limited to only 5% of the total area as per Indonesia's Public Work and Housing regulation (IESR, 2021). Subsequently, to address the challenges of dynamic nearshore water conditions, the approach for developing a PV technology floater shape must be improved.

Many prior investigations have demonstrated the numerous advantages of multihull ship designs over monohulls. This ship with several hulls is a novel type of high-speed performance ship created in the late twentieth century (Molland et al., 2011). The multihull concept originated from their ability to handle more cargo than ordinary commercial containerships, resulting in improved capacity and lower emissions due to greatly decreased water resistance. This has a positive effect on environmental conservation (Zhao et al., 2023). Figure 6 might help demonstrate specific types of high-speed and low-resistance vessels.

Figure 6. High-speed and low-resistance vessels: (a) Catamaran, (b) Trimaran, (c) Quadrimaran, (d) Pentamaran
Ref: (Dr. Hans, 2021; Schionning Designs International (Pty) Ltd, 2024; Yanuar & Waskito, 2017)

The innovative concept attempts to replicate the characteristics of high-speed boats in a stationary (non-propelled) PV floater system. However, the number of hulls utilized increases the cost component in manufacture, but this is rationalized by the size of the service deck along with the location of solar panels, where this renewable energy source is proportional to area. As explained by Bhattacharyya (1978) and (Zhao et al., 2023), the addition of lateral hulls enhances the metacenter height,

resulting in a significant reduction in excitation force due to the degree of roll motion, which is related to the natural period of the motion, lateral acceleration, and extra transverse stability.

Similar to other renewable energy technology concepts, the development of FPV technology is expected to evolve towards the concept of energy farming at sea. This involves a series of configurations, both laterally and transversally on the water surface where the incremental addition of floaters becomes inevitable. Hence, the complex and multi-analysis of CFD within fluid-structure interaction shall be conducted the key design of FPV energy farming (Wei et al., 2024).

Response Amplitude Operators (RAOs)

The results of seakeeping numerical simulations for all designs are presented in this section. Due to the symmetrical geometry in the stern and bow of all proposed floating structures, the wave heading is considered only at $\varphi = 0°$ (following sea), $\varphi = 45°$ (quartering sea), and $\varphi = 90°$ (beam sea). From the three graphs provided, it becomes demonstrated that at a 0° heading, all heave response graphs, from catamaran to pentamaran, demonstrate zero differences. This is because when waves counter from the forward position (FP) or backside (AP), the FPV structural will be move (heave response mode) in a synchronized up-and-down action. This is due to the hull configuration in the design is arranged adjacent to one another.

The response degrees at $\varphi = 45°$ and $\varphi = 90°$ are significantly lower than at $\varphi = 0°$. The trend throughout all three graphs has been described as follows: The heave response motion decreases as the wave incidence angle approaches perpendicular to the longitudinal axis of the ship's centerline ($\varphi = 90°$). This behavior is also consistent with the increase of hull types. At headings of $\varphi = 45°$ and $\varphi = 90°$, the pentamaran model demonstrates the lowest heave reaction.
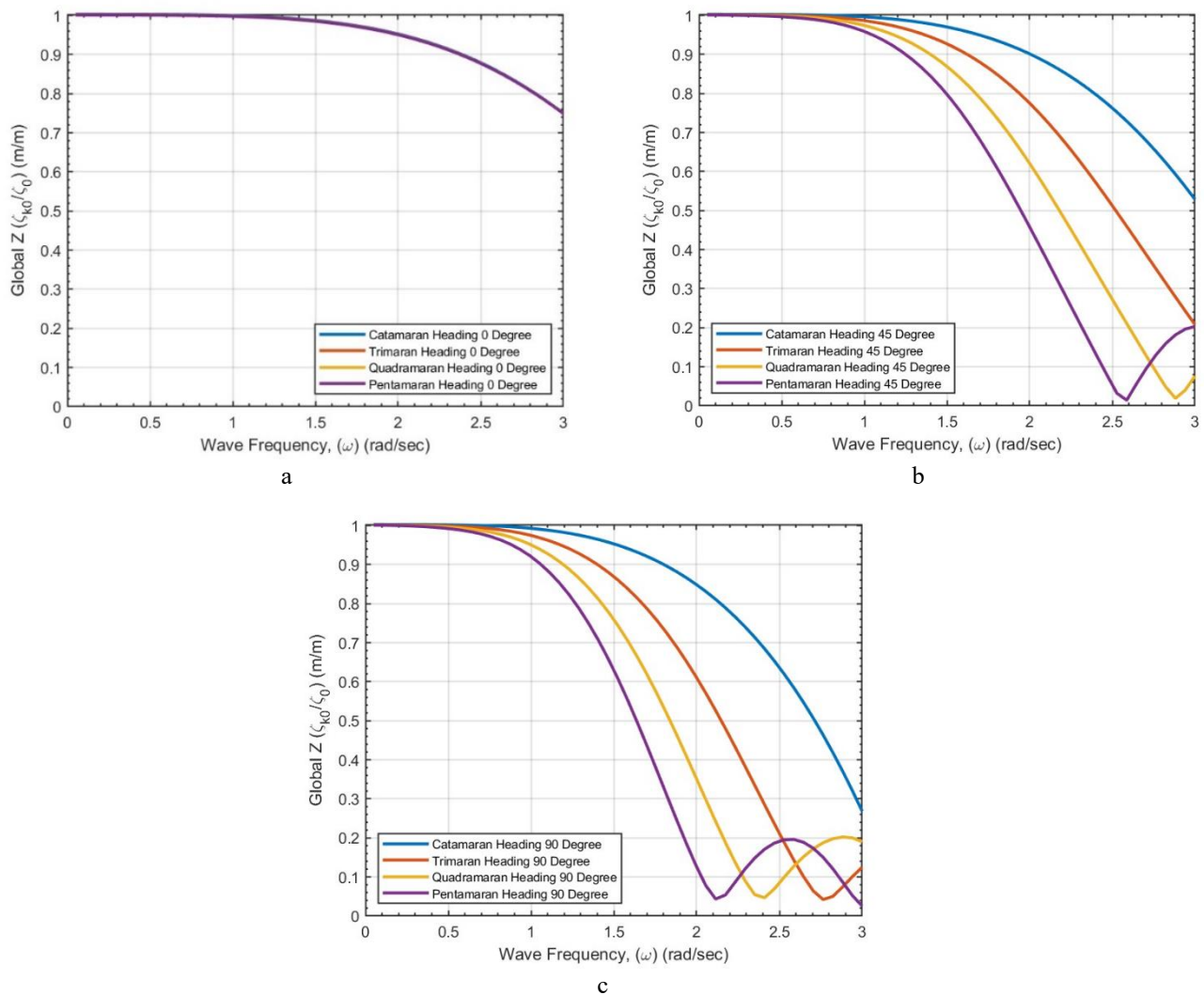

a

b

c

**Figure 7.** Heave RAO: (a) $\varphi = 0°$, (b) $\varphi = 45°$, (c) $\varphi = 90°$

Furthermore, the roll Response Amplitude Operator (RAO) curve of the FPV structure shows that the highest value of the peak roll response RAO occurs in the φ = 90° of wave incidence direction, indicating that this is the dominant direction leading to the roll response when compared to the 45° heading. Nevertheless, further investigation shows a significant discrepancy in peak values between the two headings (φ = 45 & 90°), particularly in the catamaran model (the difference can reach over 40% - nonetheless this percentage value will decrease significantly with the addition of configurations to the FPV structure). Then the addition of the hull configuration for the floater, the area under the roll motion response curve (RAO) will decrease, indicating that with an increasing number of float structure configurations, the roll motion can be dampened.
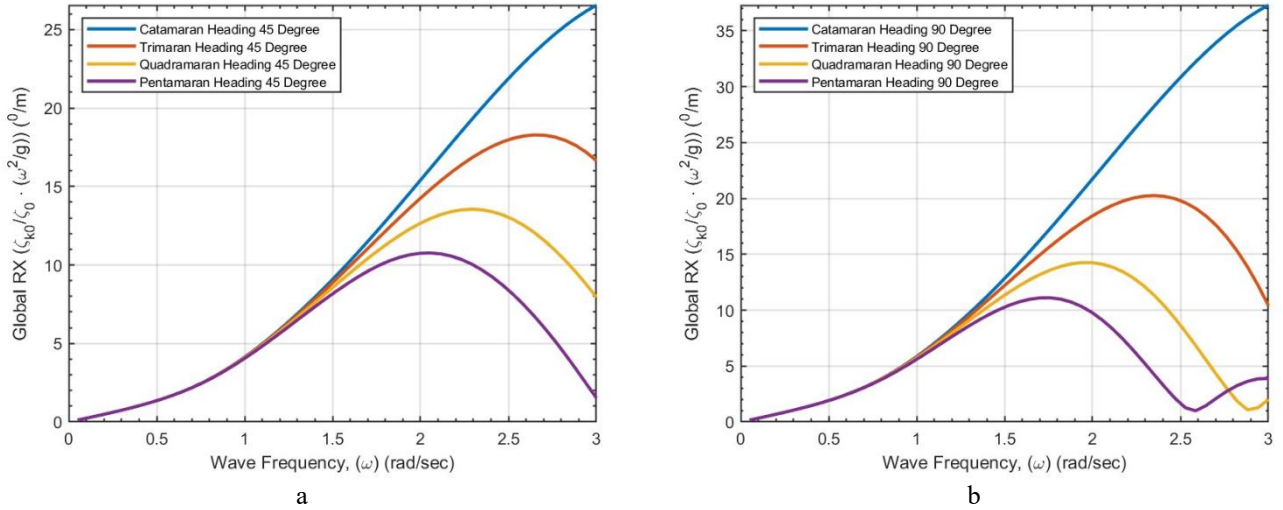
Figure 8. Roll RAO: (a) φ = 45°, (b) φ = 90°

Then, the final response considered as pure oscillatory motion is the pitch motion. The findings of this investigation are unique, considering that the pitch response at the φ = 0° heading for all proposed designs is similar to the heave motion mode (no differences occur). When the structure is stimulated by waves from the dominant pitch motion direction (φ = 0°), all models will consistently provide identical response values throughout the specified wave frequency range. This also indicates that the addition of hull configuration to the FPV structure does not have a significant influence on the performance of this pitch motion mode.

However, there is a substantial difference at 45° heading, since the consequences of adding hull configurations to the FPV structure appear to have a significant effect. The pentamaran hull configuration has the lowest peak value of the pitch Response Amplitude Operator (RAO) response when compared to the other floater configuration.
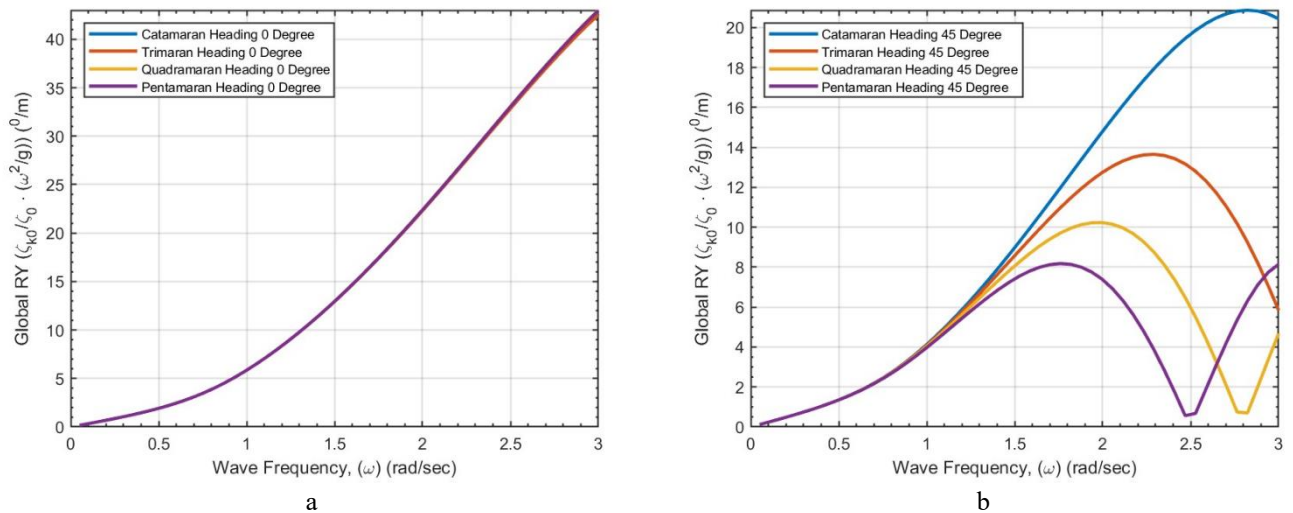

Figure 9. Pitch RAO: (a) φ = 0°, (b) φ = 45°.

Significant Response Value of Oscillatory Pure Motions

Analyzing the wave spectrum is the subsequent process in evaluating the effect of the hull configuration. Figure 10 illustrates JONSWAP's wave spectra for sea states 1–4 based on Table 7, which indicate sea conditions.

Table 7. Sea-state codes

Sea-State	Description of sea	Significant Wave Height (m)
1	Calm (rippled)	0.10
2	Smooth (wavelets)	0.50
3	Slight	1.25
4	Moderate	2.50
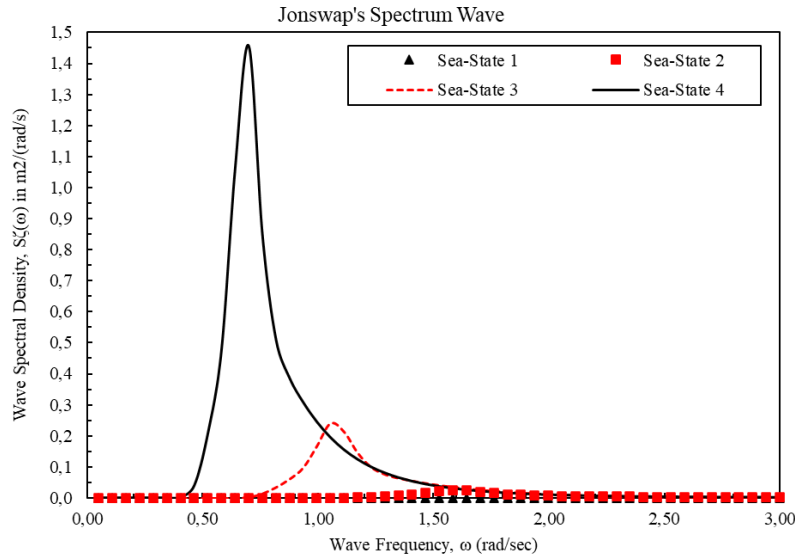
Figure 10. JONSWAP's wave spectra for various sea-state

Two key factors that influence the arrangement of response spectra are the wave spectrum and the RAO for specific modes. Moreover, stochastic parameters were computed based on the curves of response spectra for each mode. Nevertheless, the primary focus of this investigation will be restricted to determining significant response amplitudes, which represent an average measurement of the largest 33% of responses, within the sea-state range of 1-4.

Then, in Figures 11-14, it is shown that there is a negative linear trend in all three motion modes (pure oscillatory motion) when hull configurations have been added to the FPV floater structure under each sea-state scenario.

These graphs provide insightful data, particularly if there is an objective for developing an FPV floater structure using the single-array design concept with the addition of configurations laterally. The equation of each graph's negative linear regression line can be applied to predict the qualitative value of floating structure motion for an FPV structure with more than 5 hulls (pentamaran).
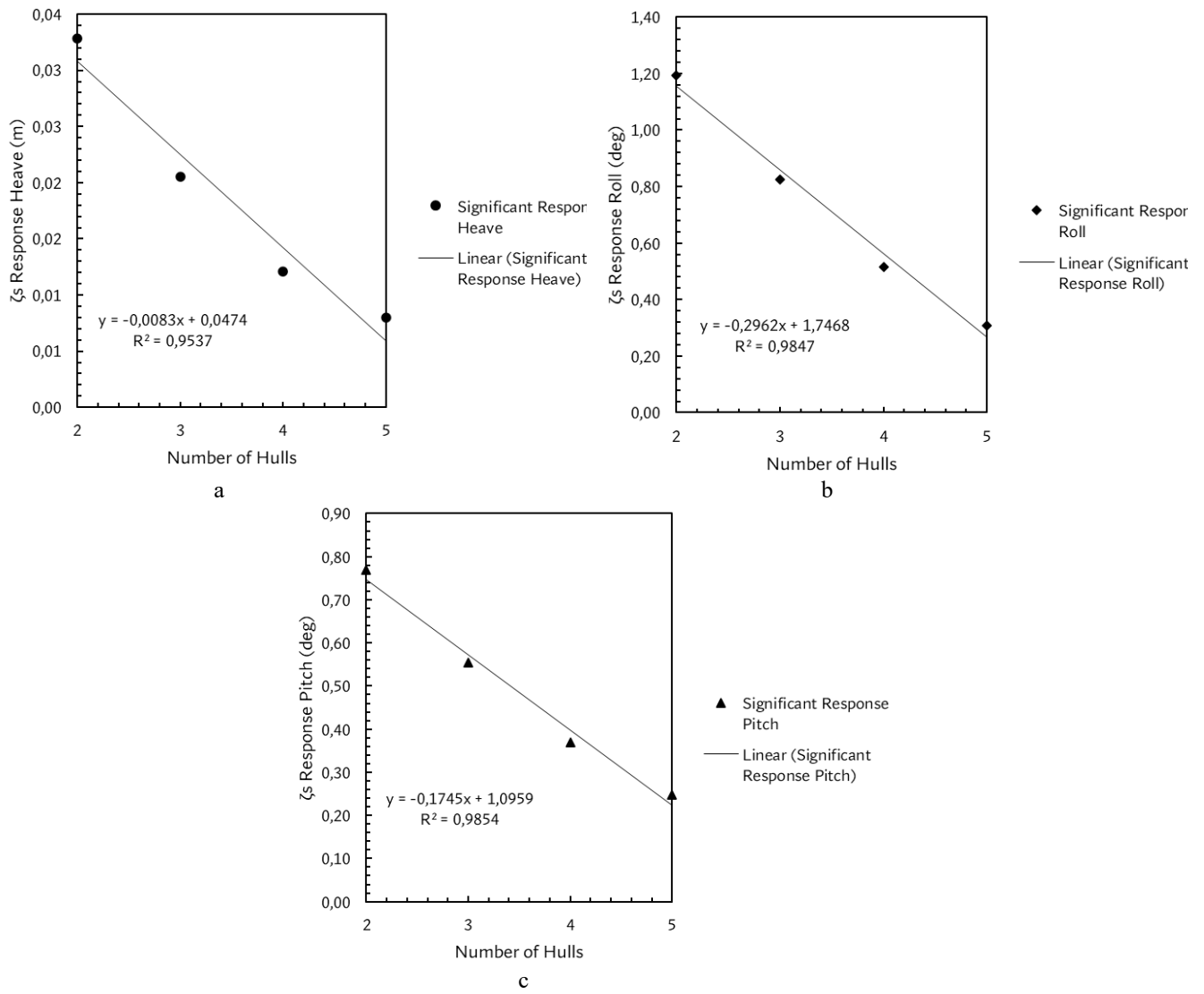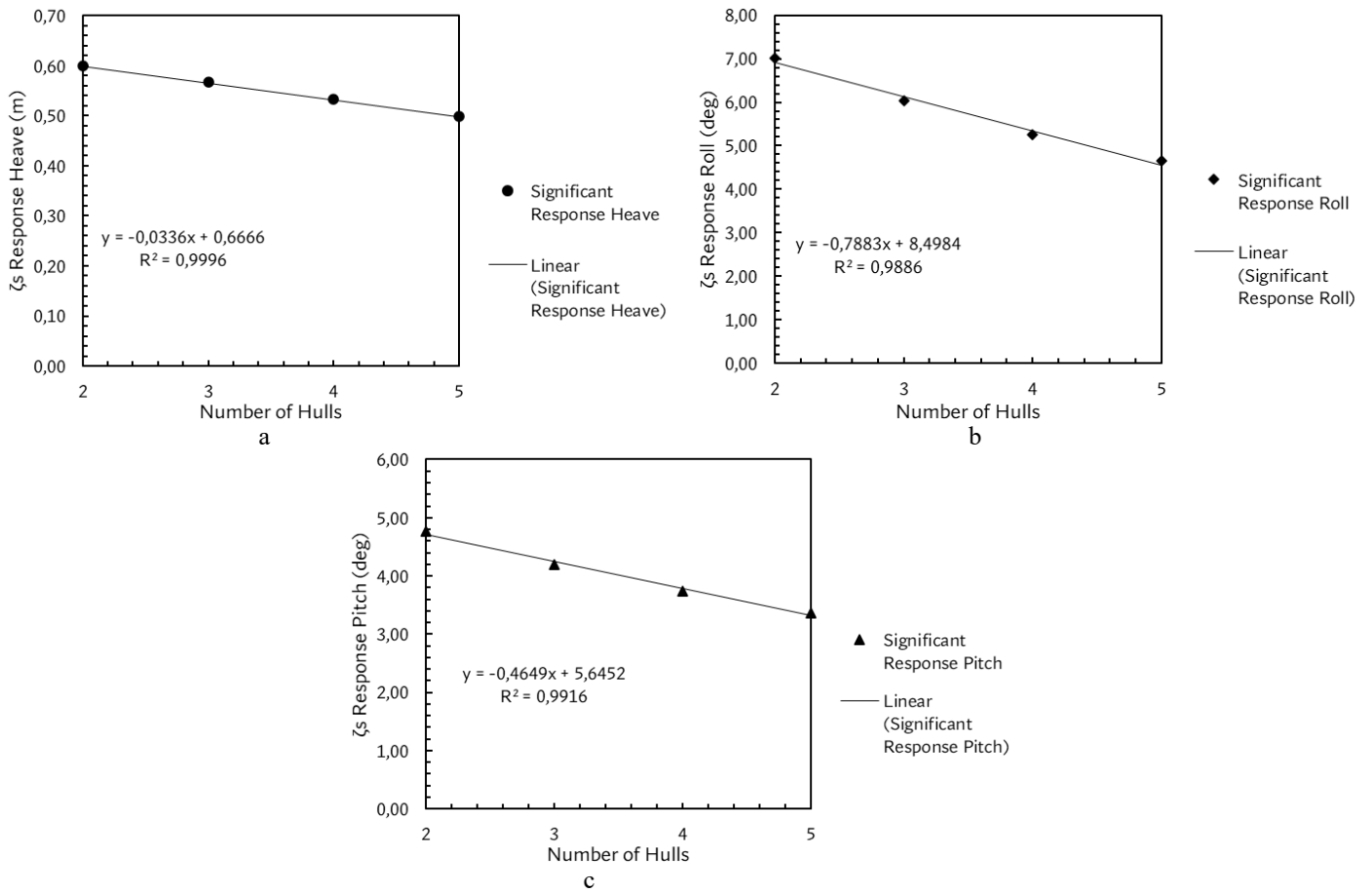
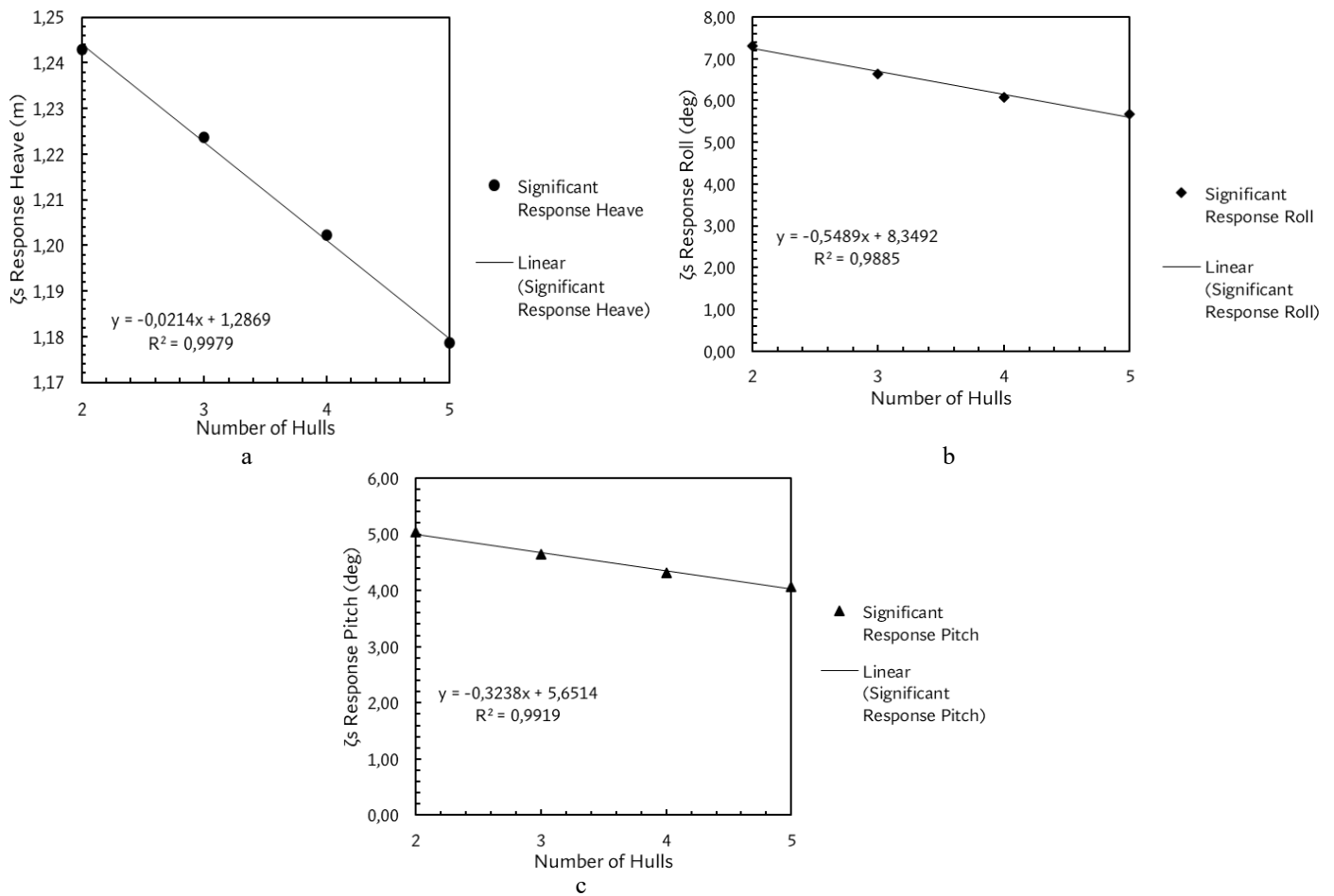**Figure 11.** ζs Respons FPV – Sea-State 1: (a) Global Z, (b) Global RX, (c) Global RY
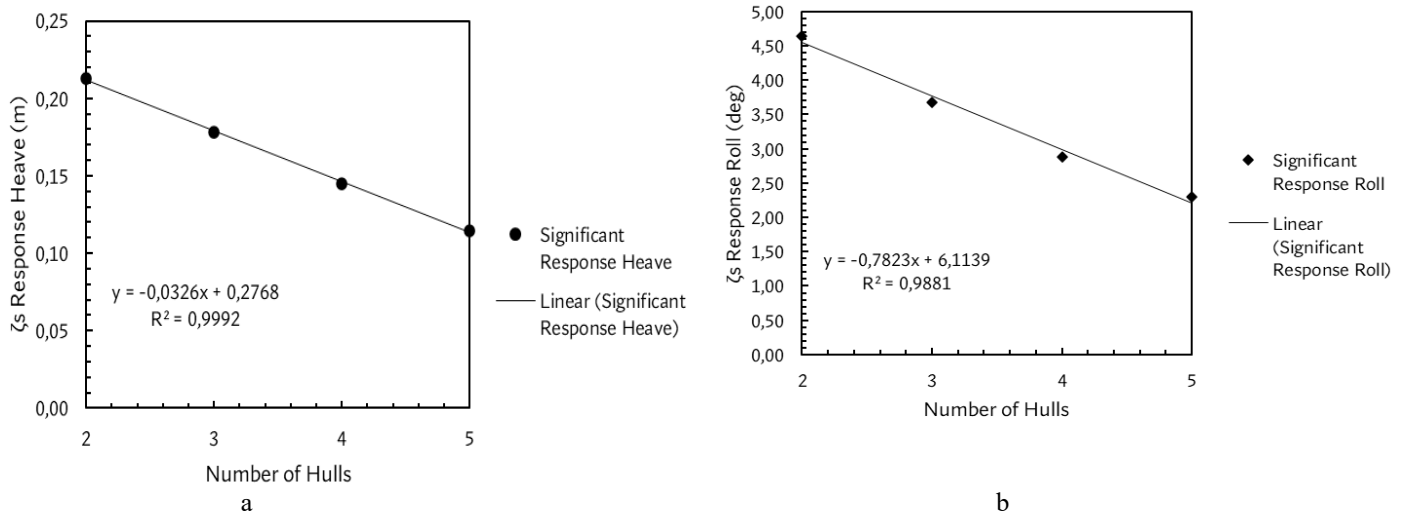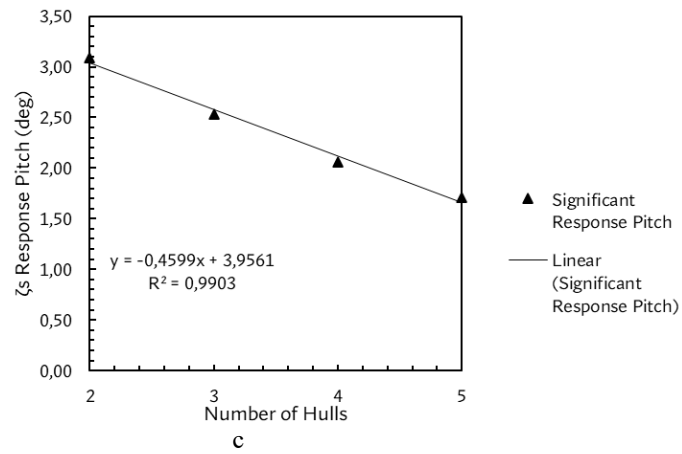
Figure 12. ζs Respons FPV – Sea-State 2: (a) Global Z, (b) Global RX, (c) Global RY

Figure 13. ζs Respons FPV – Sea-State 3: (a) Global Z, (b) Global RX, (c) Global RY

Figure 14. ζs Respons FPV – Sea-State 4: (a) Global Z, (b) Global RX, (c) Global RY

Table 8 illustrates the relationship between the variable reflecting the quantity of proposed floating structure configurations along the X-axis and its impact on the quality of each motion mode generated along the Y-axis under predefined sea-state conditions.

Table 8. Regression equation for each motion mode

Sea-State	Significant Responses	Equation	Curve Form	R^2
	Heave	y= -0.0083x + 0.0474		0.954
Sea-State 1	Roll	y= -0.2962x + 1.7468		0.985
	Pitch	y= -0.1745x + 1.0959		0.985
	Heave	y= -0.0326x + 0.2768		0.999
Sea-State 2	Roll	y= -0.7823x + 6.1139		0.988
	Pitch	y= -0.4599x + 3.9561	Linear	0.990
	Heave	y= -0.0336x + 0.6666	Negative	1.000
Sea-State 3	Roll	y= -0.7883x + 8.4984		0.989
	Pitch	y= -0.4649x + 5.6452		0.992
	Heave	y= -0.0214x + 1.2869		0.998
Sea-State 4	Roll	y= -0.5489x + 8.3492		0.989
	Pitch	y= -0.3238x + 5.6514		0.992

CONCLUSIONS

A study was conducted to investigate the impact of platform configurations and environmental conditions on the performance of floating solar photovoltaic (FPV) structures. Numerical Computational Fluid Dynamics (CFD) simulations based on 3-D

diffraction were carried out to identify pure oscillatory motions in heave, pitch, and roll for all proposed designs. The numerical findings show that the FPV structure with 5 (five) floater hulls has the lowest motion response (pure oscillatory motion) compared to other configurations under each sea-state scenario. Furthermore, there is a negative linear trend in the motion response of the FPV structure from the catamaran configuration to the pentamaran. It is essential to note that if subsequent studies desire for a concept with several hull configurations exceeding 5 hulls, the negative linear regression equations for each motion under different sea-state conditions can be predicted, provided that the design concept, geometric shape, configuration arrangement, and several control variables remain similar to this study.

Furthermore, , The future works should consider the selection of mooring configurations and various types for the FPV structure's mooring system. The hydrodynamics responses of mooring lines and FPV structures could be investigated in the time domain analysis.

DECLARATION OF GENERATIVE AI AND AI-ASSISTED TECHNOLOGIES IN WRTITING

During the preparation of this work the author(s) did not use any generative AI and AI-assisted technologies in writing of this article.

CONTRIBUTION STATEMENT

Author 1:Methodology; software; validation; formal analysis; investigation; resources; writing – original draft; writing – review & editing; visualization. **Author 2:** Validation; investigation; writing – review & editing; supervision. **Author 3:** Investigation; writing – review & editing; funding acquisition. **Author 4:** Investigation; writing – review & editing; supervision. **Author 5:** Conceptual; investigation; writing – review & editing; supervision; project administration.

ACKNOWLEDGEMENTS

REFERENCES

Allsop, W., Goff, C., Wallingford, H. R., Pullen, T., Silva, E., & Williamson, T. (2018). *Wave and overtopping predictions on reservoirs and inland waterways*. https://www.researchgate.net/publication/327405119

Amir Garanovic. (2021, July 26). *EDF to develop 240MW floating solar project in Laos*. Offshore Energy. https://www.offshore-energy.biz/edf-to-develop-240mw-floating-solar-project-in-laos/

Ansys. (2019). *Ansys Aqwa Theory Manual*.

B. Beetz. (2018). Africa Announces Utility-Scale Floating Solar Tender. *PV Magazine*. https://www.pv-magazine.com/2018/04/09/africa-announces-utility-scale-floating-solar-tender/

Bentley System. (2022). *Maxsurf Modeler User Manual*.

Bhattacharyya, Rameswar. (1978). *Dynamics of marine vehicles*. John Wiley & Sons.

Boersma, T., Van der Laan, J., Noorduyn, O., & Mesbahi, M. (2019). *A Comprehensive Overview of 200+ Global Floating Solar Plants*. Solar Plaza. https://www.solarplaza.com/channels/future-grid/12067/200-global-floating-solar-plants/

Bosma Br, Zhang Zhe, Brekken Ted K.A, Ozkan H. Tuba, Mc Natt Cameron, & C Yim Solomon. (2012). Wave Energy Converter Modeling in the Frequency Domain: A Design Guide. *IEEE*, 2099–2106.

Cazzaniga, R., Cicu, M., Rosa-Clot, M., Rosa-Clot, P., Tina, G. M., & Ventura, C. (2017). Compressed air energy storage integrated with floating photovoltaic plant. *Journal of Energy Storage*, *13*, 48–57. https://doi.org/https://doi.org/10.1016/j.est.2017.06.006

Choi, Y. K., Choi, W. S., & Lee, J. H. (2016). Empirical Research on the Efficiency of Floating PV Systems. *Science of Advanced Materials*, *8*(3), 681–685. https://doi.org/10.1166/sam.2016.2529

Claus, R., & López, M. (2022). Key issues in the design of floating photovoltaic structures for the marine environment. *Renewable and Sustainable Energy Reviews*, *164*, 112502. https://doi.org/10.1016/j.rser.2022.112502

CSI Solar Co. Ltd. (2021, January). *Preliminary Technical Information Sheet of Canadian Solar*.

Det Norske Veritas. (2010). *Recommended Practice Environmental Conditions and Environmental Loads*. http://www.dnv.com

Directorate General of Renewable Energy and Energy Conservation. (2022). *Performance Report of the Directorate General of Renewable Energy and Energy Conservation for 2022* (Vol. 1, Issue). EBTKE Directorate General . https://globalsolaratlas.info/global-pv-potential-study

Djatmiko, E. B. (2012). *The Behavior and Operability of Offshore Structure in Random Waves*. ITS Press.

Dr. Hans. (2021, July 7). *Quadramaran: what do you think?* Cruisers & Sailing Forums. https://www.cruisersforum.com/forums/f48/quadrimaran-what-do-you-think-253004.html

Emiliano Bellini. (2022, January 7). *Chinese fish pond hosts 550 MW solar farm*. PV Magazine. https://www.pv-magazine.com/2022/01/07/chinese-fish-pond-hosts-550-mw-solar-farm/

Enerdata. (2020, April 23). *Chenya Energy reaches financial close for 181 MW floating PV park (Taiwan)*. Enerdata. https://www.enerdata.net/publications/daily-energy-news/chenya-energy-reaches-financial-close-181-mw-floating-pv-park-taiwan.html

Frost&Sullivan. (2024). *Global Solar Photovoltaic Growth Opportunities*. Frost&Sullivan Online Store. https://store.frost.com/global-solar-photovoltaic-growth-opportunities.html

Gudrun Sigtryggsdottir, F. (2022). *Environmental loads on embankment dams in mountainous regions*. www.nve.no

Haug, Ø., Trym, L., & Sjøberg, S. (2018). *Evaluation and Comparison of Operability and Operational Limits of Service Vessel Designs in Exposed Aquaculture*.

IEA. (2022). *International Energy Agency for Methane Tracker*. IEA. https://www.iea.org/data-and-statistics/data-tools/methane-tracker-data-explorer#comparison-sources

IESR. (2021). *Technical Potential of Floating Solar Photovoltaic in Central Java*. IESR. https://www.iea.org/reports/solar-pv

IESR. (2022). *Indonesia Energy Transition Outlook 2023: Tracking Progress of Energy Transition in Indonesia: Pursuing Energy Security in the Time*.

Islam, M. I., Maruf, M. H., Al Mansur, A., Ashique, R. H., Asif ul Haq, M., Shihavuddin, A. S. M., & Jadin, M. S. (2023). Feasibility analysis of floating photovoltaic power plant in Bangladesh: A case study in Hatirjheel Lake, Dhaka. *Sustainable Energy Technologies and Assessments*, *55*. https://doi.org/10.1016/j.seta.2022.102994

Japan International Cooperation Agency (JICA). (2020). *The Study on Power Network System Master Plan in Lao People's Democratic Republic*. https://openjicareport.jica.go.jp/pdf/12328027_01.pdf

Korea Energy Agency. (2022). *National Survey Report of PV Power Applications in Korea*. https://iea-pvps.org/wp-content/uploads/2024/01/IEA-PVPS-National-Survey-Report-KOREA-2022.pdf

Lindholm, D., Selj, J., Kjeldstad, T., Fjær, H., & Nysted, V. (2022). CFD modelling to derive U-values for floating PV technologies with large water footprint. *Solar Energy*, *238*, 238–247. https://doi.org/10.1016/j.solener.2022.04.028

Liu, H., Krishna, V., Lun Leung, J., Reindl, T., & Zhao, L. (2018). Field experience and performance analysis of floating PV technologies in the tropics. *Progress in Photovoltaics: Research and Applications*, *26*(12), 957–967. https://doi.org/10.1002/pip.3039

Liu, H., Kumar, A., & Reindl, T. (2020). *The Dawn of Floating Solar—Technology, Benefits, and Challenges* (pp. 373–383). Springer Link. https://doi.org/10.1007/978-981-13-8743-2_21

Masdar. (2023). *Cirata Floating Solar Photovoltaic*. Masdar. https://masdar.ae/en/news/newsroom/president-of-indonesia-inaugurates-floating-solar-plant

Minister of Energy and Mineral Resources of the Republic of Indonesia. (2021). *Electricity Supply Business Plan* (Vol. 1). State Electricity Company (PT. PLN).

Mittal, D., Saxena, B. K., & Rao, K. V. S. (2017). Floating solar photovoltaic systems: An overview and their feasibility at Kota in Rajasthan. *2017 International Conference on Circuit ,Power and Computing Technologies (ICCPCT)*, 1–7. https://doi.org/10.1109/ICCPCT.2017.8074182

Molland, A. F., Turnock, S. R., & Hudson, D. A. (2011). *Ship Resistance and Propulsion : Practical Estimation of Ship Propulsive Power*. Cambridge University Press.

Oliveira-Pinto, S., & Stokkermans, J. (2020). Assessment of the potential of different floating solar technologies – Overview and analysis of different case studies. *Energy Conversion and Management*, *211*, 112747. https://doi.org/10.1016/j.enconman.2020.112747

Pimentel Da Silva, G. D., & Branco, D. A. C. (2018). Is floating photovoltaic better than conventional photovoltaic? Assessing environmental impacts. *Impact Assessment and Project Appraisal*, *36*(5), 390–400. https://doi.org/10.1080/14615517.2018.1477498

Presidential Regulation 112/2022, Pub. L. No. 112, Presidential Regulation of the Republic of Indonesia 1 (2022).

Reuters. (2021, July 22). *Sunseap to build $2 billion floating solar farm in Indonesia, world's largest*. Reuters. https://www.reuters.com/business/energy/sunseap-build-2-bln-floating-solar-farm-indonesia-worlds-largest-2021-07-22/

Rosa-Clot, M., Rosa-Clot, P., Tina, G. M., & Scandura, P. F. (2010). Submerged photovoltaic solar panel: SP2. *Renewable Energy*, *35*(8), 1862–1865. https://doi.org/10.1016/j.renene.2009.10.023

Rosa-Clot, M., & Tina, G. M. (2018). Submerged PV Systems. *Submerged and Floating Photovoltaic Systems*, 65–87. https://doi.org/10.1016/B978-0-12-812149-8.00004-1

Sahu, A. K., & Sudhakar, K. (2019). Effect of UV exposure on bimodal HDPE floats for floating solar application. *Journal of Materials Research and Technology*, *8*(1), 147–156. https://doi.org/10.1016/J.JMRT.2017.10.002

Schionning Designs International (Pty) Ltd. (2024). *Tracer 1500TRi Preliminary Study Plans*. https://schionningdesign.com/sdi/

Sen, D., Sharma, P., & Muni, B. (2015). DESIGN PARAMETERS OF 10KW FLOATING SOLAR POWER PLANT. *International Advanced Research Journal in Science, Engineering and Technology*, *2*(1). https://doi.org/10.17148/IARJSETP10

Shi, W., Yan, C., Ren, Z., Yuan, Z., Liu, Y., Zheng, S., Li, X., & Han, X. (2023). Review on the development of marine floating photovoltaic systems. *Ocean Engineering*, *286*. https://doi.org/10.1016/j.oceaneng.2023.115560

Silalahi, D. F., Blakers, A., Stocks, M., Lu, B., Cheng, C., & Hayes, L. (2021). Indonesia's vast solar energy potential. *Energies*, *14*(17). https://doi.org/10.3390/en14175424

Silalahi, D. F., Gunawan, D., Wahyuni, E., Dipayana, G. F., Hardhi, M., Winofa, N. C., Ramadhan, R. A., & Hidayat, T. (2022). Indonesia Post-Pandemic Outlook: Strategy towards Net-Zero Emissions by 2060 from the Renewables and Carbon-Neutral Energy Perspectives. In *Indonesia Post-Pandemic Outlook: Strategy towards Net-Zero Emissions by 2060 from the Renewables and Carbon-Neutral Energy Perspectives*. Penerbit BRIN. https://doi.org/10.55981/brin.562

Sreenath, S., Sudhakar, K., Yusop, A. F., Solomin, E., & Kirpichnikova, I. M. (2020). Solar PV energy system in Malaysian airport: Glare analysis, general design and performance assessment. *Energy Reports*, *6*, 698–712. https://doi.org/10.1016/j.egyr.2020.03.015

Suastika, K., Silaen, A., Aliffrananda, M. H. N., & Hermawan, Y. A. (2021). Seakeeping analysis of a hydrofoil supported watercraft (Hysuwac): A case study. *CFD Letters*, *13*(5), 10–27. https://doi.org/10.37934/cfdl.13.5.1027

T. Kenning. (2018). *Independent power producer (IPP) Akuo Energy has started construction of a 17MW O'MEGA1 floating solar plant in France*. NS Energy. https://www.nsenergybusiness.com/news/akuo-energy-floating-solar-plant-france/

Tom Kenning. (2019, June 13). *Thai utility readies tender for 45MW floating solar on Sirindhorn Dam*. PV-Tech. https://www.pv-tech.org/egat-readies-tender-for-45mw-floating-solar-at-sirindhorn-dam/

Trapani, K., & Redõn Santafé, M. (2015). A review of floating photovoltaic installations: 2007-2013. In *Progress in Photovoltaics: Research and Applications* (Vol. 23, Issue 4, pp. 524–532). John Wiley and Sons Ltd. https://doi.org/10.1002/pip.2466

Wang, J., & Lund, P. D. (2022). Review of Recent Offshore Photovoltaics Development. In *Energies* (Vol. 15, Issue 20). MDPI. https://doi.org/10.3390/en15207462

Wei, Y., Zou, D., Zhang, D., Zhang, C., Ou, B., Riyadi, S., Utama, I. K. A. P., Hetharia, W., Wood, T., & Huang, L. (2024). Motion characteristics of a modularized floating solar farm in waves. *Physics of Fluids*, *36*(3). https://doi.org/10.1063/5.0199248

World Bank Group, E. and S. (2019). *Where Sun Meets Water: Floating Solar Handbook for Practitioners*. World Bank. www.worldbank.org

Yanuar, & Waskito, K. T. (2017). Experimental study of total hull resistance of pentamaran ship model with varying configuration of outer side hulls. *Procedia Engineering*, *194*, 104–111. https://doi.org/10.1016/j.proeng.2017.08.123

Zhao, B., Jiang, H., Sun, J., & Zhang, D. (2023). Research on the Hydrodynamic Performance of a Pentamaran in Calm Water and Regular Waves. *Applied Sciences (Switzerland)*, *13*(7). https://doi.org/10.3390/app13074461